Ab initio simulations of molten Ni alloys

Christopher Woodward,[1,a)] Mark Asta,[2] Dallas R. Trinkle,[3] James Lill,[4] and Stefano Angioletti-Uberti[5]
[1]*Materials and Manufacturing Directorate, Air Force Research Laboratory, Wright Patterson Air Force Base, Dayton, Ohio 45433-7817, USA*
[2]*Department of Materials Science and Engineering, University of California, Berkeley, California 94720, USA and Department of Chemical Engineering and Materials Science, University of California at Davis, Davis, California 95616, USA*
[3]*Department of Materials Science and Engineering, University of Illinois, Urbana-Champaign, Urbana, Illinois 61801, USA*
[4]*High Performance Technologies Inc., Wright Patterson Air Force Base, Dayton, Ohio 45433-7817, USA*
[5]*Department of Materials, Imperial College London, Prince Consort Road 20, SW72BP London, United Kingdom*

(Received 17 March 2010; accepted 2 May 2010; published online 4 June 2010)

Convective instabilities responsible for misoriented grains in directionally solidified turbine airfoils are produced by variations in liquid–metal density with composition and temperature across the solidification zone. Here, fundamental properties of molten Ni-based alloys, required for modeling these instabilities, are calculated using *ab initio* molecular dynamics simulations. Equations of state are derived from constant number-volume-temperature ensembles at 1830 and 1750 K for elemental, binary (Ni–X, X=Al, W, Re, and Ta) and ternary (Ni–Al–X, X=W, Re, and Ta) Ni alloys. Calculated molar volumes agree to within 0.6%–1.8% of available measurements. Predictions are used to investigate the range of accuracy of a parameterization of molar volumes with composition and temperature based on measurements of binary alloys. Structural analysis reveals a pronounced tendency for icosahedral short-range order for Ni–W and Ni–Re alloys and the calculations provide estimates of diffusion rates and their dependence on compositions and temperature. © *2010 American Institute of Physics*. [doi:10.1063/1.3437644]

The constant pressure to improve efficiency and performance of terrestrial and aero turbine engines has produced significant materials and engineering challenges. The components that see the highest temperatures, turbine airfoils, are actively cooled through internal channels and employ thermal barrier coatings that insulate the base alloy from the highest gas flow temperatures. Modern airfoils are manufactured by a directional solidification process that produces a single crystal Ni-based superalloy component with unrivaled high temperature properties. Superalloy chemistries and airfoil geometries have become increasingly complex with each generation of aero turbine engine design. While the evolving chemistry has produced significant improvements in high temperature creep resistance, the increased levels of refractory elements are also associated with the formation of defects during processing. These so-called freckle defects are formed by density-driven convective instabilities in the solidification front (i.e., the mushy zone) that result in chains of small equiaxed grains. The high angle grain boundaries and compositional variations produced by these defects are known to adversely affect mechanical properties. Quantitative models for predicting the conditions leading to the formation of these defects are required for optimizing the materials processing of these materials for high performance applications.

Currently there is also a strong desire in the aerospace material and design communities to move toward a systems design approach that would enable optimization of the site specific properties of a component. The balance of material and component properties could then take advantage of variations in the processing-structure-properties relationships of the material and the site specific requirements of the part. For single-crystal Ni-based superalloys this will require a quantitative model for predicting commercial processing regimes for defect-free casting over the widest possible range of refractory metal compositions. Current theory of thermochemical convection in the mushy zone suggests that such instabilities occur when a Rayleigh number exceeds a critical value.[1–4] The Rayleigh number (R) is a measure of the ratio of the buoyancy force to the retarding frictional force in the mushy zone

$$R = (\Delta\rho/\bar{\rho})gKl/\alpha\nu, \tag{1}$$

where l is an appropriate length scale, K is the average permeability, g the acceleration produced by gravity, α is the thermal diffusivity, ν is the kinematic viscosity of the fluid, and $(\Delta\rho/\bar{\rho})$ is the density contrast. This last term is a measure of the variation in mass density over the mushy zone between the liquid metal near the solid–liquid dendrite interface and the cooler melt at the bottom and sides walls of the mold. Temperature gradients present during casting as well as the variations in solute concentration in the melt that develop as a consequence of equilibrium partitioning between solid and liquid phases will influence the density contrast. The mass-density difference reflects both the composition (c) and temperature (T) dependence of the liquid-phase molar

a)Electronic mail: christopher.woodward@wpafb.af.mil.

volume $V(c,T)$. Freckle formation is highly susceptible to variations in the permeability of the mushy zone as dictated by dendrite arm spacing as well as the density contrast. Traditional models of the Rayleigh-number criterion assume that the density gradients are aligned with solidification front and in the plane normal to the acceleration provided by gravity. These assumptions have become problematic as airfoil designs have become more complex with the introduction of cooling channels and other design features. Currently, most castings have significant heat losses through the mold that create horizontal thermal gradients and tilted solid–liquid interfaces.

Confirming mathematical models for freckle formation in specific alloy systems requires accurate assessment of the various parameters in Eq. (1). The kinematic viscosity, permeability, and density gradients are difficult to measure experimentally and are not well documented for superalloys. The present work is part of a larger effort to better quantify the parameters defining this Rayleigh number. Others in our research team have estimated the permeability using fluid flow simulations of the mushy zone.[5] Such calculations use realistic reconstructions of the mushy-zone dendritic structure derived from serial sectioning of decanted molds.[6] Documented here are ongoing efforts to develop and validate robust models for the liquid metal densities, $\Delta\rho$, using *ab initio* molecular dynamics (AIMD) simulations.[7]

In a detailed study of superalloy liquid metal densities Mukai *et al.*[8–10] measured the densities of several binary liquid Ni-based alloys, and a few representative ternaries, as functions of c and T. These data were then used to develop a model for $V(c,T)$ in superalloys.[10] Because of the lack of sufficient data for multicomponent systems, the model approximates the total molar volume as the sum of solute partial molar volumes which are derived from constituent binary systems. Changes in $V(c,T)$ driven by the explicit interactions between the different chemical species (e.g., solutes) are neglected. Also, measured density data for some key elements, such as Re, were unavailable. The partial molar volume contributions for these elements were treated as parameters to fit available data from multi-component superalloys. Nevertheless, predictions from the Mukai model produce good agreement, within a few percent, with the available experimentally measured densities of commercial superalloys.

In this manuscript comparisons with models fit to experimental measurements will focus mostly on the recent parameterization by Mukai.[10] However, we note that an earlier parameterization that was developed by Sung *et al.*[11] has found widespread use in the community. In this paper we focus on comparisons of the AIMD data with the more recent parameterization of Mukai *et al.* which is based on a more extensive database of measured densities, including most of the binary systems considered in our work.

Experimental measurements of the composition and temperature dependent densities for either model (NiAlW) or multicomponent superalloys (i.e., RENE-N4) relevant to our larger effort on freckle formation are not readily available. In the current work we use state-of-the-art AIMD simulations as a means for testing the accuracy of the Mukai model for $\rho(c,T)$ in this system. These calculations are useful as an independent test the accuracy of the Mukai parameters for elements and ranges of composition where direct measurements of liquid density are unavailable.

I. COMPUTATIONAL METHODS

In this work AIMD is used to compute time-averaged properties of molten Ni-based alloys. The simulation method evolves ionic positions using classical Nosé–Hoover dynamics yielding trajectories that sample an equilibrium distribution corresponding to an ensemble with fixed particle number, volume, and temperature (i.e., *NVT*) with interatomic forces derived from the electronic structure approximation provided by density functional theory (DFT). The commercial DFT software Vienna *ab initio* simulation package (VASP),[12–14] developed at the Institut für Materialphysik of the Univerität Wien, is used to generate Hellmann–Feynman (i.e., atomic) forces required for the AIMD study.

The liquid-alloy simulations employed a 500-atom cubic supercell with periodic boundary conditions and fixed periodic lengths. AIMD calculations were performed for elemental, binary, and ternary alloy compositions, twelve in all, at two simulation temperatures. The alloy compositions are tailored to the test the accuracy of the Mukai parameterization and its application to Ni–Al–W alloys used as model materials in validation experiments. The calculations also sample alloy chemistries containing refractory additions, such as Re, where experimental data is currently unavailable. Within the manuscript the composition of the simulation cells are identified by the number of each atomic species in the calculation such as: Al_{500}, Ni_{500}, $Ni_{400}Al_{100}$, $Ni_{473}W_{27}$, $Ni_{400}W_{100}$, $Ni_{473}Re_{27}$, $Ni_{400}Re_{100}$, $Ni_{473}Ta_{27}$, $Ni_{400}Ta_{100}$, $Ni_{436}Al_{50}W_{14}$, $Ni_{436}Al_{50}Re_{14}$, and $Ni_{436}Al_{50}Ta_{14}$.

The Nosé–Hoover equations of motion were integrated using thermostat temperatures of $T=1830$ and 1750 K. To ensure that the conserved energy in the Nosé–Hoover dynamics produce a drift in time no larger than 1 meV/atom ps time steps (Δt) for the MD simulations were chosen at or below $\Delta t=0.003$ ps. Initial configurations for the Ni_{500} and $Ni_{400}Al_{100}$ simulations were derived from snapshots of classical molecular dynamics simulations based on classical interatomic potentials.[15] For the binary and ternary alloy simulations the initial configurations were obtained by replacing Ni and Al atoms, selected at random, by the appropriate target atomic species. Different temperature simulations were then started from the same atomic configurations with different random initial velocities.

The self-consistent charge density and corresponding interatomic forces were computed at each time step to integrate the ionic trajectories. Also, relevant system properties including the pressure, energy, temperature, and atomic coordinates were calculated and stored. The calculations employed a plane-wave basis set with a cutoff energy of 260 eV to represent the electronic wave functions and ultrasoft pseudopotentials.[16,17] For simulations of this size a single k-point (Γ) was more than adequate for performing accurate reciprocal-space summations. Electronic eigenvalues are occupied according to Fermi statistics with an electronic tem-

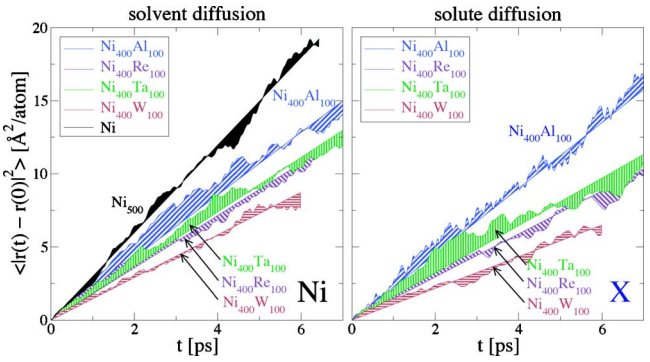

FIG. 1. (Color online) Calculated AIMD mean-square displacements of solvent (left) and solute (right) species for elemental Ni and binary Ni–X (X =Al, W, Re, and Ta) alloys at 1830 K. Deviations in the "random walk" from the long-time linear diffusion relation, $\langle|r(t)-r(0)|^2\rangle=6Dt$, are shown as filled areas for each species. The results shown here are from the lowest pressure simulations at these chemistries. The diffusion constants (d) in Table I are derived from the slopes of the mean-square displacement curves at several volumes interpolated to zero pressure. Self diffusion of Ni decreases with solute additions with Al producing the smallest effect and W the largest. The relative solute diffusion in these liquid Ni–X metals follows the same trends of the respective solvent diffusion.

perature equal to that for the ionic system. Also, the exchange correlation potential was approximated using a generalized-gradient approximation (PW91).[18] For each temperature and alloy composition at least three simulations were performed over a range of volumes spanning plus or minus 5% of the estimated equilibrium value. In order to obtain good statistical precision in calculated equation of state parameters total simulation times ranged from 5–10 ps. Correlation times for pressure, energy, and temperature were found in the range of 40–60 fs, and this was taken into account for all thermal averages and error estimates. Diffusion and liquid structure factors were calculated in order to verify that the sizes of the supercells and simulation times were of sufficient magnitude to produce realistic results.

II. RESULTS

While the main focus of this study is the prediction of liquid metal molar volumes, the AIMD calculations also provide a means to quantify the local ordering and kinetics in the melt. Such observations are also used to establish that the simulations are of long enough duration to allow appreciable interdiffusion such that the calculated thermal averages are not biased by the choice of the initial atomic configuration. Also, the cell volume must be large enough such that positional correlations decay sufficiently over the length of the simulation box in order to produce a realistic liquid structure. These convergence requirements are considered before reviewing the calculated dependence of molar volume on composition and temperature.

A. Kinetics

In order to estimate the values of the diffusion kinetics in these systems the averaged mean-squared displacements for Ni, Al, W, Ta, and Re were calculated from the simulations of the pure and binary liquids. Figure 1 shows the solvent and solute results for Ni, and binary $Ni_{400}X_{100}$(X =Al, W, Ta, Re) liquids at $T=1830$ K for the lowest pressure *NVT* simulations for each chemistry. The slopes of the best-fit lines relating mean-square displacements and time are used to derive the estimates of the concentration-dependent tracer diffusion constants at this temperature. As previously found in atomistic simulations of liquid metals, before producing diffusive motion, the mean squared displacements exhibit a ballistic trajectory.[19] The AIMD simulations at these temperatures produce an initial ballistic regime of approximately 0.3 ps. However, we find that because this regime is small compared to the scale of the entire simulation time, the changes introduced by the first 0.3 ps of data is significantly less than the overall statistical errors in the final diffusion rate. All reported results in this work are fit to time periods after an initial thermalization period, typically less than 0.1 ps. Quantities in Table I are derived from the mean-squared displacements at three to four volumes and linear fits of diffusion constants with volume to compute the diffusion constants at equilibrium. The slope of this line also yields a measure of the activation volume at zero pressure as shown in the table. The self diffusion in Ni is in good agreement with a previous AIMD VASP study by Jakse and coworkers looking at the dynamic properties of liquid Ni.[20]

TABLE I. Calculated diffusion parameters (10^{-5} cm^2/s) and activation volumes for binary Ni alloys at 1830 K. Values for D are the result of a linear fit of the diffusion parameters found for the three or more calculations used to determine the equilibrium volume. The fit produces D at zero pressure and its the first derivative which is used to define the activation volume, $V_a=-k_BTd(\ln D)/dP$. Errors, in parentheses, are derived using standard propagation of errors based on the statistical error estimates from the raw data and represent estimated 95% confidence intervals on the last digit.

Composition		Solvent (Ni)		Solute (X)	
Cell	Alloy	D(Ni)	V_a(Ni)	D(X)	V_a(X)
Ni_{500}	Ni	5.3(3)	1.3(3)		
$Ni_{473}Re_{27}$	Ni–5.4Re	5.0(2)	1.3(2)	3.6(4)	0.3(5)
$Ni_{473}Ta_{27}$	Ni–5.4Ta	4.6(1)	1.3(2)	3.7(3)	0.5(4)
$Ni_{473}W_{27}$	Ni–5.4W	4.2(2)	1.3(2)	3.6(4)	0.9(6)
$Ni_{400}Al_{100}$	Ni–20Al	3.4(4)	1.2(2)	3.5(3)	2.3(4)
$Ni_{400}Re_{100}$	Ni–20Re	3.2(2)	0.9(2)	2.3(2)	0.8(3)
$Ni_{400}Ta_{100}$	Ni–20Ta	3.5(1)	1.2(2)	2.9(2)	0.9(4)
$Ni_{400}W_{100}$	Ni–20W	3.2(1)	1.1(2)	2.5(3)	1.1(2)

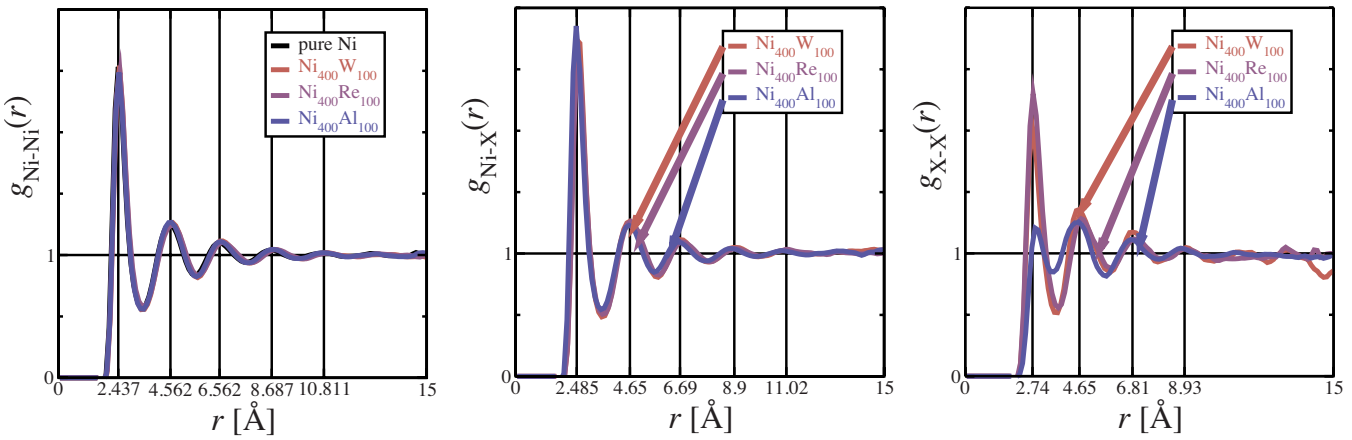

FIG. 2. (Color online) Radial distribution functions calculated from AIMD simulations for elemental Ni and binary Ni–X (X=Al, W, and Re) alloys at T =1830 K. The results shown here are from the lowest pressure simulations at these chemistries. The three plots show results, from left to right, for solvent–solvent (Ni–Ni), solvent–solute (Ni–X), and solute–solute (X–X) pairs.

Working with a 108 atom supercell at 1850 K with *NVT* sampling they find a self diffusion of 4.4×10^{-5} cm^2/s. The current simulations show Re and W as the slowest diffusion species, consistent with their large atomic mass and size, as compared to the other atomic species. Also, the Ni diffusion constant is lower in the Ni–X melts, relative to pure Ni, an effect which is roughly linear with solute concentration. However, this appears contary to the fact that the average atomic volume is larger in the alloys. Further analysis (below) reveals relatively strong solute–solvent interactions in the alloy melts, an observation which is corroborated in the radial distribution and neighbor analysis.

Classical experimental measurements of self-diffusion in liquid metals, such as capillary-reservoir or diffusion couple methods, are problematic in Ni alloys due to the lack of specific radio-isotopes.[21] Recently, because of interest in short-range ordering in Al rich Al–Ni binaries, inelastic neutron scattering has been used to study diffusion and chemical ordering in Al–Ni melts. Using these methods Chathoth *et al.*[22] measured self diffusion of 3.8×10^{-5} cm^2/s for elemental Ni at 1795 K. In another related manuscript,[23] using the same method, this group reports Ni self diffusion at 1795 K in Ni–25Al (at. %) of 3.9×10^{-5} cm^2/s. These values are in excellent agreement with our calculated values of Ni self diffusion for elemental Ni and Ni–20Al at 1830 K, $5.3(3)\times10^{-5}$ cm^2/s and $3.4(4)\times10^{-5}$ cm^2/s, respectively. There are very few measurements of solute diffusion in liquid melts, however, recently tracer diffusion constants have been reported for Ni–2W (at. %).[24] These experiments were performed in the temperature range of 1755–2022 K and were carefully designed to minimize effects of convection. The measured tracer diffusion coefficient for W, $2.4(2)\times10^{-5}$ cm^2/s, is again in excellent agreement with our results for a $Ni_{473}W_{27}$ alloy at 1830 K where we find a value of $3.6(4)\times10^{-5}$ cm^2/s.

Figure 1 and the good statistics of the interdiffusion constants demonstrates that significant interdiffusion is occurring over the timescale of the AIMD simulations and that simulations of this size, run for approximately 5–7 ps, have evolved over sufficiently long times to give robust estimates of the equilibrium molar volumes. This expectation is supported by the relatively small estimated statistical uncertainties in the molar volumes quoted below. Finally, this is also supported by the results of a test performed for binary Ni–W samples, where two different initial atomic configurations were used to compute the equilibrium volume of the same chemistry. The final results were found to agree within statistical uncertainties.

B. Local ordering

Figure 2 shows the radial distribution functions, $g_{\alpha,\beta}(r)$, for each of the (α,β) pairs of species in pure Ni and binary $Ni_{400}X_{100}$ (X=Al, W, and Re) melts. All the distribution functions converge to the uncorrelated limit of unity in a distance which is less than half the diagonal distance across the simulation cell. This verifies that the cell dimensions are large enough to provide uncorrelated motion of individual and groups of atoms. The distribution functions also provide insights into the nature of chemical ordering in the melt. For example, the main peak of g_{Ni-X} is larger than the solute–solute (X–X) and solvent–solvent (Ni–Ni) pairs which suggests a preference in the melt for chemical short-range ordering between neighbors of unlike species. Also, the average nearest-neighbor bond length for Ni–Ni and X–X bond lengths (roughly 2.59 Å) is significantly larger than for Ni–X pairs (approximately 2.485 Å). These results are consistent with a significant preference for chemical short-range ordering between Ni and X species in each of the systems considered. Information about the liquid structure beyond those given by the pair distribution function $g(\mathbf{r})$ can be obtained through the so-called common neighbor analysis (CNA) (Ref. 25) and the angle probability distribution function $P(\theta)$.

In the CNA each pair of neighbors is characterized by a triplet jkl describing the local configuration of the pair. The index j gives the number of neighbors common to both atoms in the pair, k is the number of bonds between these neighbors, and l is the longest continuous chain formed by the k bonds between common neighbors. Atoms are considered bonded (i.e., neighbors) if their separation distance falls below some critical value, typically this is taken as either the

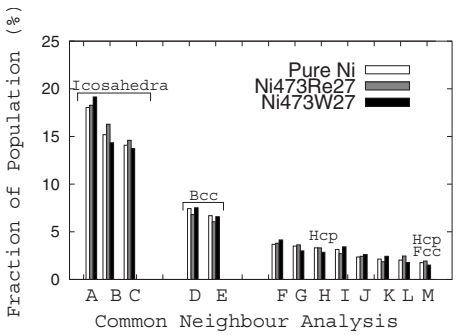

FIG. 3. CNA of pure Ni, $Ni_{473}Re_{27}$, and $Ni_{473}W_{27}$ at 1830 K. The combined analysis shows the presence of similar short-range order in the three samples, with almost no dependence on composition. Icosahedral and bcc type ordering are found to be the most abundant.

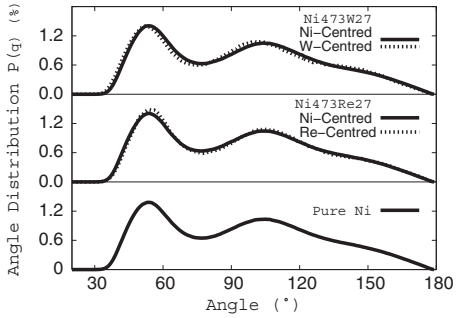

FIG. 4. Angle distribution function $P(\theta)$ at 1830 K for pure Ni, $Ni_{473}Re_{27}$, and $Ni_{473}W_{27}$. For perfect icosahedric or bcc like structures the two main peaks are expected to be around 60° and 108°, in our samples distortions due to the liquid nature shift the peaks to lower values. The angle distribution for all three cases of the Ni-centered data fall on essentially the same line, and there is a slight shift to lower angles for the W centered distribution relative to the rest of the data.

position of the first peak or the first minimum in $g(\mathbf{r})$. Here, we choose the minimum in the $g(\mathbf{r})$ as the relevant criterion. Note that in a binary or multicomponent alloy the minimum of the partial pair distribution function for the specific atoms involved is used. The CNA analysis has been performed for pure Ni, $Ni_{473}Re_{27}$, and $Ni_{473}W_{27}$ at a temperature of 1830 K and the results are shown in Fig. 3.

Figure 3 shows that there is a clear preference for the formation of icosahedral short-range order, with a secondary preference for bcc type order. A much lower distribution of fcc and hcp type clusters are found even though Ni is a closed packed metal in the solid state. It is worth noting that no clear effect of alloying with Re and W is visible in our data. This icosahedral short-range order was postulated by Frank over 50 years ago for fcc metals[26] and was recently confirmed in experimental observations for both pure liquid Ni (Ref. 27) and in Ni–Ag amorphous alloys.[28] Similar results had already been found for liquid Ni by Posada-Amarillas and Garzon[29] using a semiempirical n-body potential. Icosahedral ordering in liquid alloys of fcc metals is thought to be present because it maximizes the *short-range* density of a structure[26] (while fcc-packing maximizes the long range density[30]), thus lowering the enthalpy of the system. This type of ordering cannot be found in crystals simply because it does not permit periodic filling of a 3D space (but is commonly found in quasicrystals, for example). Presence of bcc type ordering is also interesting. Some simulations in simple Lennard–Jones systems[31] show that at moderate undercooling precritical nuclei have a preeminently bcc structure which *partially* disappear in critical nuclei.

Complimentary information about the local environment in the liquid is gained by analyzing the angle probability distribution function $P(\theta)$. $P(\theta)$ is defined so that $P(\theta)d\theta$ is the probability of finding a triplet of neighbors with an angle in the range $[\theta-\theta+d\theta]$. The $P(\theta)$ for the three different compositions that we analyzed are generally not geometrically perfect, even though the corresponding icosahedral and bcc short-range order is clearly demonstrated by the CNA analysis. For a perfect icosahedral or bcc cluster one expects bond angles of approximately 60° and 108°. As shown in Fig. 4, the shift in the peaks in the angular distribution function to slightly lower angles reflects the distortions inherent in the local structural units. While all of the Ni-centered data falls on the same line, the solute centered data for W and Re exhibit a splitting toward lower and higher angles, respectively.

C. Molar volumes

In order to compute equilibrium molar volumes using *NVT* dynamics AIMD simulations were performed at each composition for a series of simulation cell volumes where the average pressure (P) as a function of V was calculated. For each temperature and composition a total of three to four volumes were considered. The calculated time-averaged pressures were then used to derive an equation of state, assuming a quadratic relationship between P and V. Using the derived equation of state, the equilibrium (zero pressure) volume (V_0), bulk modulus $[B=-V_0(dP/dV)]$, and its pressure derivative (B') were computed. An example of this approach is shown schematically in Fig. 5 for simulations of liquid $Ni_{400}Al_{100}$ at 1830 K. The pressure is plotted, on the left-hand image, as a function of simulation time for each of the considered atomic volumes. At each volume there is an initial pressure transient, lasting for a few tenths of a picoseconds, after which the pressure fluctuates about a well defined average value indicated by the solid line. The time scale and amplitude of these fluctuations about equilibrium were used to derive estimates of the statistical uncertainties in the calculated time-averaged pressure. The right-hand side of Fig. 5 shows the results of such analysis. The data points and error bars show the pressures and associated statistical uncertainties computed as a function of volume from the AIMD simulations. Finally, the smooth solid line connecting these data points is a least-squares quadratic fit, which yields the equilibrium values of volume (V_0) and the bulk modulus as shown in the inset. Similar results are recorded in Table II, listing calculated equilibrium volumes for each of the twelve liquid Ni-based alloy compositions considered to date.

III. DISCUSSION

As described in the Introduction, a primary motivation for the present work is to use AIMD simulations as a framework for developing and validating predictive models for $\rho(c,T)$ in Ni-based superalloys. To that end listed along side

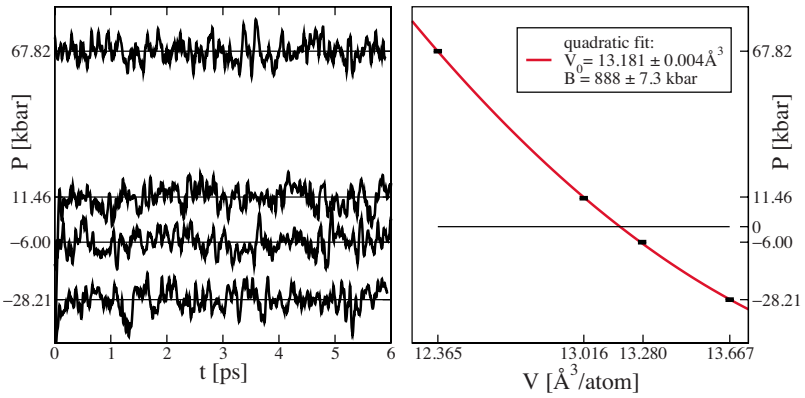

FIG. 5. (Color online) Graphic representation of the equation of state calculations for liquid metal $Ni_{400}Al_{100}$ alloy at 1830 K. Representative AIMD calculations of pressure as a function of simulation time for four volumes (left) with a horizontal line indicating time-averaged values. The volume at these pressures, with error bars, (right) are fit to a quadratic polynomial, with results of this least-squares fit shown in inset. Interpolating to the zero pressure volume produces the predicted equilibrium volume the bulk modulus and its derivative for a given composition and temperature. Error bars and estimated uncertainties are based on standard uncertainty analysis.

the AIMD results in Table II are the values from the most recent parameterization of molten superalloy densities, due to Mukai *et al.*[10] In order to produce this parameterization Mukai measured the density of elemental Ni,[8] and a wide variety of binary Ni–X alloys. Some of these compositions correspond to those considered in this study, so comparison to these measurements provides a means to gauge the accuracy of the AIMD simulations. For elemental Ni at these temperatures the error is 1.6% and 0.8% for 1750 K and 1830 K, respectively. Using Mukai's fits to experimental measurements for Ni–19.7Al and Ni–5.83W (at. %), the approximate compositions for the first two binaries listed in Table II, we find average errors in the AIMD results to be below 1.8%. There are also several other recent measurements of liquid Ni alloy densities. Using a sessile drop method Feng *et al.*[32] measured the density of elemental Ni and dilute solutions of W in Ni. The AIMD predictions are within 1.4% of the elemental Ni results. Also, Plevachuk and co-workers have developed a noncontact technique which uses electromagnetic levitation and optical dilatometry to measure the high temperature liquid metal densities. Their recent measurements focused on the Al rich Ni–Al alloys, however extrapolating our Ni–20Al predictions to the measured density at Ni–25Al we find the AIMD prediction within 0.6% of the measured values.[33] The AIMD results for molar volumes are consistently larger than the measured values, with the exception of this noncontact method. While this trend is similar to the predictions of traditional density functional methods (i.e., applications of the local density approximation) for crystal lattice parameters, we note that these calculations are based on the generalized-gradient approximation (PW91).[18]

For compositions in the range of the original Mukai parameterization, based on partial molar volumes, interpolations to quaternary and higher order systems are reported to have errors in the range of 2%. In order to illustrate the trend in the molar volume data the AIMD and Mukai results are plotted in Fig. 6. For compositions inside the range of Mukai's experimental database the agreement between the two methods is within 2%, as indicated in Fig. 6 by the dotted lines. However, when the model needs to extrapolate to the AIMD sampled compositions errors can be quite large, as is the case for $Ni_{400}W_{100}$, $Ni_{473}Ta_{27}$, and $Ni_{400}Re_{100}$. Also for the case of $Ni_{400}Ta_{100}$, not shown in Fig. 6, the Mukai parameterization diverges from the AIMD result by at least 7 cm^3/mole. There is also a systematic increase in the difference between the fitted and AIMD results with decreasing temperature, as indicated by the spread of data points within

TABLE II. Calculated atomic volumes (cm^3/mole) and volumetric thermal expansion coefficients (10^{-5} K^{-1}) for molten Ni alloys at 1750 and 1830 K. The numbers in parentheses represent estimated 95% confidence intervals on the last digit. The calculated (AIMD) results are compared with the predictions of the parameterized model due to Mukai *et al.*[10] For the Ni–Ta alloys Mukai fit to compositions in the dilute limit (<3.5 at. %) making it inappropriate to extrapolate to high solute concentrations.

	T=1750 K				T=1830 K			
	AIMD		Mukai		AIMD		Mukai	
Composition	V	β	V	β	V	β	V	β
Al_{500}	12.80(2)	12.0			12.91(3)	10.9		
Ni_{500}	7.57(1)	7.10	7.4597	18.6	7.62(1)	6.71	7.5724	18.6
$Ni_{400}Al_{100}$	7.88(1)	7.33	7.7628	13.9	7.94(1)	5.55	7.8492	13.8
$Ni_{473}W_{27}$	7.66(1)	6.61	7.5534	16.3	7.70(1)	5.74	7.6520	16.1
$Ni_{400}W_{100}$	7.94(1)	6.38	6.5192	155.	7.98(1)	6.44	7.3294	138.
$Ni_{473}Re_{27}$	7.65(1)	7.37	7.4940	26.0	7.69(1)	7.00	7.6499	25.5
$Ni_{400}Re_{100}$	7.91(1)	6.84	7.5869	44.9	7.93(1)	6.25	7.8593	43.3
$Ni_{473}Ta_{27}$	7.70(1)	7.28	7.3310	29.7	7.75(1)	6.26	7.5053	29.0
$Ni_{400}Ta_{100}$	8.14(1)	10.5	···		8.18(1)	9.09	···	
$Ni_{436}Al_{50}W_{14}$	7.77(1)	7.52	7.6920	12.0	7.80(1)	6.18	7.7655	11.8
$Ni_{436}Al_{50}Re_{14}$	7.75(1)	7.62	7.6291	20.0	7.80(1)	9.10	7.7510	19.7
$Ni_{436}Al_{50}Ta_{14}$	7.79(1)	7.74	7.6911	10.4	7.84(1)	7.29	7.7553	10.4

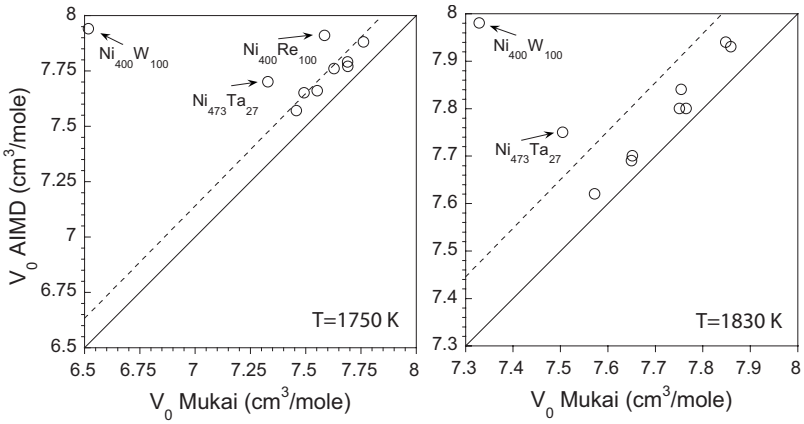

FIG. 6. Comparison of molar volumes calculated with AIMD simulations and estimated using the Mukai parameterization. Data in perfect agreement would fall on the line representing a slope of one, the dashed line indicates where the two results differ by 2%. The outliers are compositions that fall outside the composition ranges included in the fit of the Mukai model.

the 2% margin of error. As discussed below this is an indication that the two methods produce different coefficients of thermal expansion.

The ternary alloys in Table II can also be used to assess the accuracy of the experimental parameterization for interpolating within the sampled experimental data and the sensitivity of the approximation for predicting molar volumes for compositions outside the range of experimentally fitted data. The former case is a test of approximating the molar volume as the sum of partials molar volumes of noninteracting chemical species. For example, each of the ternary alloy compositions $Ni_{436}Al_{50}X_{14}$ with refractory elements (X=W, Re, or Ta) can be represented as the average of the binary $Ni_{400}Al_{100}$ and $Ni_{473}X_{27}$ melts also considered here. This composition relationship is equivalent to traversing from the Ni–Al to Ni–X sides of a ternary triangle [i.e., inset in Fig. 7(a)]. As illustrated in Fig. 7(a) the AIMD simulations produce molar volumes of the ternary melts that are all very well approximated (to within 0.8%) by a linear interpolation between the binary alloy values. The Mukai model is also accurate using the average of the two binaries, producing less than a 0.4% deviation from linearity for the ternary alloys containing W and Re. However, the molar volume predicted by the Mukai model for $Ni_{473}Ta_{27}$ produces deviations from linearity of approximately 2% and 3% for the ternary and binary alloys respectively.

Figure 7(b) illustrates the variation in molar volume for Ni–W and Ni–Re for solute concentrations up to 20 at. %. The AIMD results produce nearly linear behavior (though not plotted similar results are found for Ni–Ta alloys) in this range of composition. The Mukai parameterization produces significant deviations from linearity for the Ni–W alloys ($\approx$13%). Surprisingly the Re predictions, which are not fit to binary data but are inferred from measurements of multicomponent alloys, show linear behavior in agreement with the AIMD results. Mukai's predictions for the Ni–Ta alloys are not included here because the extrapolation from 4 to 20 at. % produces deviations from linearity of more than 100%. These results suggest that one of the main assumptions in the Mukai parameterization, namely that the partial molar volumes of the binary alloys can be used to *interpolate* molar volumes for multicomponent systems, is reasonably accurate in the Ni–Al–X (X=W, Re, or Ta) alloys. The AIMD results

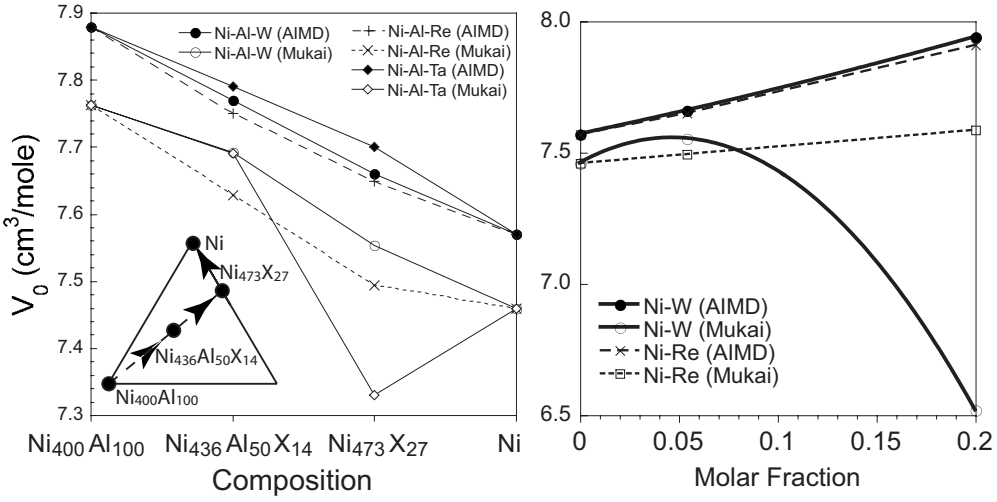

FIG. 7. Variation in molar volumes at 1750 K for ternary and binary alloys calculated using AIMD simulations and estimated using the Mukai parameterization. The figure on the left shows compositions spanning the ternary triangle (see inset). Results are linear in composition with deviations from linearity of less than 0.8%. The Mukai model results for $Ni_{473}Ta_{27}$ are the exception producing deviations from linearity of approximately 3%. The figure on the right shows binary Ni–X (X=W and Re) compositions up to Ni–20X at. % which is outside the range of the Mukai reference measurements. The Mukai Ni–W molar volumes show significant deviations from linearity, which is not predicted by the AIMD simulations. Similar, though far more dramatic deviations are observed for Ni–Ta alloys in this range of composition.

illustrate that application of the Mukai model should be restricted to the range of compositions sampled by the underlying experimental measurements.

Four of the compositions at 1750K, calculated using AIMD, fall close to or within the range of compositions fit using multilinear regression by Sung *et al.*[11] Differences in molar volumes between the two methods range from one to nine percent with a standard deviation of five percent. The AIMD results are in better agreement with the Mukai parameterization based on this small data sample.

Variations in molar volume with temperature for alloys with high solute concentrations can be derived from the AIMD results using one of several methods. Liquid metal density measurements in binary Ni alloys indicate that the temperature dependence is linear so finite difference methods should be reasonably accurate. An alternative technique, based on the results of AIMD simulations at a single temperature, was used to derive the thermal expansion coefficient (β) for the temperatures and compositions listed in Table II. For any ensemble averaged property $\langle A\rangle$ in a canonical ensemble

$$\langle A\rangle = \frac{\Sigma_i A_i \exp(-E_i/k_B T)}{\Sigma_i \exp(-E_i/k_B T)}, \tag{2}$$

where E is the energy of the system. Taking the derivative with temperature and using correlation notation, $[A,B] = \langle AB\rangle - \langle A\rangle\langle B\rangle$

$$\frac{d\langle A\rangle}{dT} = \frac{[\langle AE\rangle - \langle A\rangle\langle E\rangle]}{k_B T^2} = \frac{[A,E]}{k_B T^2}, \tag{3}$$

substituting the ensembled averaged pressure for $\langle A\rangle$ gives: $d\langle P\rangle/dT = [P,E]/(k_B T^2)$. The volumetric temperature expansion coefficient can be expressed as

$$\beta = \frac{1}{V_0}\frac{dV_0}{dT} = \left.\frac{1}{V_0}\frac{dV_0}{dP}\frac{dP}{dT}\right|_{V_0}. \tag{4}$$

Using the definition of the bulk modulus: $B = 1/V_0 dP/dV|_{V_0}$, where, consistent with the current notation, P is the system pressure as apposed to the applied pressure

$$\beta = \left.\frac{1}{B}\frac{dP}{dT}\right|_{V_0} = \frac{[P,E]_{V_0}}{k_B T^2 B}. \tag{5}$$

All the quantities in the last equation are readily available for each composition and temperature sampled by the AIMD calculations and the predicted values for β are shown in Table II. Using the value of β at one temperature to estimate the molar volume at the other temperature for each table entry yields predictions with average errors of approximately 0.1%.

Comparing the AIMD values for β to that measured by modified sessile drop and modified pycnometric methods[10] we see that the AIMD results consistently underestimate these thermal expansion coefficients. Table II shows Mukai's prediction of the coefficient of thermal expansion and we note that for the compositions actually measured the agreement of the AIMD results is at best within a factor of two. Mukai's experimental measurements using the (modified) sessile drop method and (modified) pycnometric method estimate β for elemental Ni as 1.8×10^{-4} K^{-1}. Previous studies using a wider variety of methods[21,34] estimate β for elemental Ni to be in the range of $1.-1.5\times10^{-4}$ K^{-1}. Also, one earlier study based on gamma ray attenuation,[35] an experimental method for measuring liquid metal densities not influenced by surface tension or chemical contamination on the fluid surface, found the coefficient of thermal expansion for elemental liquid Ni of 9.42×10^{-5} K^{-1}. The only other noncontact method density measurement technique that has been applied to the Ni alloys is the very recent work of Plevachuk *et al.* where using electromagnetic levitation and optical dilatometry they find a coefficient of thermal expansion of 1.2×10^{-4} K^{-1} for Ni–25Al (at. %). This compares very well with Mukai's most recent work in Ni–Al alloys, where using a modified sessile drop method[36] he estimates the CTE of this alloy to be 1.32×10^{4} K^{-1}. In general the AIMD results are in better agreement with the results of noncontact density experiments, such as gamma ray attenuation and electromagnetic levitation/optical dilatometry techniques, though here also the computational method underestimates β by approximately 25% for elemental Ni.

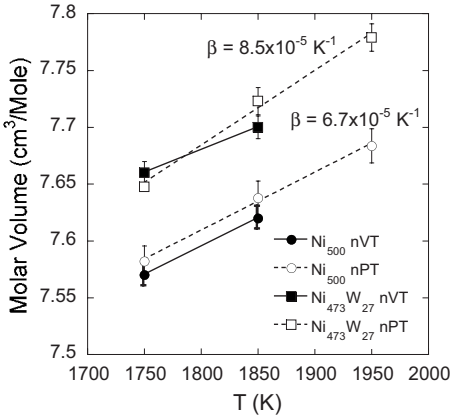

FIG. 8. The variation in molar volume with temperature for elemental Ni and $Ni_{473}Al_{27}$ calculated using *NVT* and *NPT* ensembles. The coefficient of thermal expansion ($\beta = V^{-1}dV/dT$), calculated from a linear fit to each data set, are shown adjacent to each curve. The two methods for deriving the molar volume are within numerical error of the respective calculations, producing slopes, and β that are also within numerical error.

In order to better characterize the coefficient of thermal expansion the temperature dependence of the molar volumes was studied over a wider range of temperatures using a version of VASP that was modified to sample constant number-pressure-temperature (*NPT*) statistics.[37] The results of calculations, for elemental Ni and $Ni_{473}W_{27}$ at 1750, 1850, and 1950 K, are shown in Fig. 8. Within the error of the respective calculations the *NVT* and *NPT* ensembles give the same molar volumes for a given chemistry and temperature. The wider temperature range of the *NPT* calculations also yields values for β, as indicated in Fig. 8, that are consistent with the previous calculations. We conclude that though the results are self-consistent at this level of approximation the AIMD are at best underestimating the coefficient of thermal expansion by 25%.

Another measure of the self consistency between AIMD calculations and the Mukai model are the predictions for par-

TABLE III. Partial molar volumes at infinite dilution.

Chemistry		T=1750 K		T=1850 K	
Solute	PMV	AIMD	Mukai	AIMD	Mukai
W	$\bar{V}^{\infty}_{W}/V_{Ni}$	1.25	1.55	1.24	1.33
Re	$\bar{V}^{\infty}_{Re}/V_{Ni}$	1.22	1.08	1.20	1.19
Ta	$\bar{V}^{\infty}_{Ta}/V_{Ni}$	1.38	2.13	1.37	1.61

tial molar volumes in the limit of dilute solute concentrations. For a binary alloy the methods of intercepts implies that the partial molar volume for a solute is $\bar{V}_{solute}=V+(1-c)dV/dc$, where c is the solute concentration. In the dilute limit as $c\rightarrow 0$ the reference volume, V, becomes the molar volume for pure Ni, V_{Ni}. The resulting estimates of the partial molar volumes at infinite dilution, $\bar{V}^{inf}_{solute}/V_{Ni}$, calculated from the AIMD results and the Mukai parameterization are given in Table III. Conventional thermodynamics would suggest that $\bar{V}^{inf}_{solute}/V_{Ni}$ would be somewhat insensitive to changes in temperature ($T>T_{melt}$), and this weak dependence is observed in the raw experimental data for Ni–W.[8] The Mukai model predicts large changes in partial molar volume at small solute concentrations, an effect that is particularly pronounced in Ni–Ta. Such results are consistent with small errors in the second order fitting coefficients introduced in the quadratic fits to the narrow range of experimentally measured compositions. Such errors would also produce large excursions in liquid metal densities for high solute concentrations shown in Fig. 7. The AIMD results predict very small changes with temperature of the partial molar volumes in the dilute limit. This is an area of research that warrants further study given the limited experimental data in the dilute limit.

IV. CONCLUSION

AIMD calculations were used to estimate the molar volume of a variety of liquid metal alloys, including both elemental Al and Ni, three Ni–X binary, and three Ni–Al–X (X=Al,W,Re,Ta) ternary alloys. The AIMD results consistently over estimate the molar volumes, typically by less than 2%, when compared to experimental measurements using methods where there is contact between the Ni liquid and a surface or containment vessel. Better agreement is found with noncontact experiments, though the available data in the range of compositions considered in this study is quite limited. Overall the molar volumes are in very good agreement with available experimental density measurements and produce self-consistent variations in molar volumes as a function of chemistry and temperature for the binary and ternary alloys considered. The AIMD results are also in reasonable agreement with numerical fits for complex molar volume chemistries that are based on the results of density measurements in binary alloys.[10] However, when such models are required to extrapolate to chemistries outside the measured range of solute concentrations they do not provide an accurate assessment of liquid metal densities.

Coefficients of thermal expansion were derived from both changes in molar volume with temperature and the pressure and energy dependence at a single temperature. While the two methods produce statistically equivalent coefficients of thermal expansion, the calculated values are consistently smaller than that observed experimentally. Noncontact density measurements are in better agreement with the current AIMD results. An extension of the VASP method was implemented that allows for *NPT* ensembles. Applications of this method to a subset of the chemistries and temperatures studied using *NVT* statistics verified the derived trends in molar volumes with chemistry and temperature. Results for the two methods were found to be within statistical error of the underlying simulations.

The molecular dynamics calculations also produce a wealth of other information about the kinetics and ordering of these liquid metal alloys. Diffusion parameters were predicted for the solvent and solutes in elemental Ni and seven binary Ni–X (X=Al,Re,Ta,W) alloy compositions and excellent agreement was found with recent diffusion measurements in Ni, Ni–Al, and Ni–W. Due to the rapid diffusion rates in the molten state, AIMD simulation offer a reasonable means for estimating diffusivities in liquid alloys and offers an alternative to the high temperature diffusion experiments.

ACKNOWLEDGMENTS

This research was supported in part by a grant of computer time from the DoD High Performance Computing Modernization Program at the Air Force Research Laboratory DoD Supercomputing Research Center (AFRL-DSRC). MA and DRT were supported in part with a grant from the Air Force Office of Scientific Research under the Materials Engineering for Affordable New Systems (MEANS-II) program. The authors gratefully acknowledge insightful discussions with T. Pollock, P. Voorhees, O. Senkov, and S.H. Davis, and the technical assistance provided by S. Kajihara at the AFRL-DSRC.

[1] J. R. Sarazin and A. Hellawell, Metall. Mater. Trans. A **19**, 1861 (1988).
[2] T. M. Pollock and W. H. Murphy, Metall. Mater. Trans. A **27**, 1081 (1996).
[3] P. Auburtin, S. L. Cockcroft, and A. Mitchell, in *Superalloys 1996*, edited by R. Kissinger, D. Deye, D. Anton, A. Cetel, M. Nathal, T. Pollock, and D. Woodford (TMS, Warrendale, Pennsylvania, 1996), p. 433.
[4] C. Beckermann, J. P. Gu, and W. J. Boettinger, Metall. Mater. Trans. A **31**, 2545 (2000).
[5] S. M. Roper, S. H. Davis, and P. W. Voorhees, Metall. Mater. Trans. A **38**, 1069 (2007).
[6] J. Madison, J. E. Spowart, D. J. Rowenhorst, J. Fiefler, and T. M. Pollock, *Proceedings of the Eleventh International Symposium on Superalloys* (The Minerals, Metals and Materials Society, Warrendale, Pennsylvania, 2008) pp. 881–888.

[7]C. Woodward, M. Asta, J. Lill, D. Trinkle, and S. Angioletti-Uberti, *Proceedings of the HPCMP Users Group Conference 2008* (Conference Publishing Services, Los Alamitos, California, 2008) pp. 169–174.
[8]K. Mukai, L. Fang, and Z. Li, Mater. Trans. **45**, 1754 (2004).
[9]K. Mukai, Z. Li, and L. Fang, Mater. Trans. **45**, 2987 (2004).
[10]K. Mukai, Z. Li, and K. C. Mills, Metall. Mater. Trans. B **36**, 255 (2005).
[11]P. K. Sung, D. R. Poirier, and E. McBride, Mater. Sci. Eng., A **231**, 189 (1997).
[12]G. Kresse and J. Hafner, Phys. Rev. B **47**, 558 (1993).
[13]G. Kresse and J. Hafner, Phys. Rev. B **49**, 14251 (1994).
[14]G. Kresse and J. Furthmüller, Phys. Rev. B **54**, 11169 (1996).
[15]M. Asta, D. Morgan, J. J. Hoyt, B. Sadigh, J. D. Althoff, D. de Fontaine, and S. M. Foiles, Phys. Rev. B **59**, 14271 (1999).
[16]D. Vanderbilt, Phys. Rev. B **41**, 7892 (1990).
[17]G. Kresse and D. Joubert, Phys. Rev. B **59**, 1758 (1999).
[18]J. P. Perdew and Y. Wang, Phys. Rev. B **45**, 13244 (1992).
[19]X. Han, M. Chen, and Y. Lü, Int. J. Thermophys. **29**, 1408 (2008).
[20]N. Jakse, J. F. Wax, and A. Pasturel, J. Chem. Phys. **126**, 234508 (2007).
[21]T. Iida and R. Guthrie, *The Physical Properties of Liquid Metals* (Clarendon, Oxford, 1988).
[22]S. M. Chathoth, A. Meyer, M. M. Koza, and F. Juranyi, Appl. Phys. Lett. **85**, 4881 (2004).
[23]S. K. Das, J. Horbach, M. M. Koza, S. M. Chatoth, and A. Meyer, Appl. Phys. Lett. **86**, 011918 (2005).
[24]J. P. Leonard, T. J. Renk, M. O. Thompson, and M. J. Aziz, Metall. Mater. Trans. A **35**, 2803 (2004).
[25]J. Honeycutt and H. Andersen, J. Phys. Chem. **91**, 4950 (1987).
[26]F. Frank, Proc. R. Soc. London, Ser. A **215**, 43 (1952).
[27]G. W. Lee, A. K. Gangopadhyay, K. F. Kelton, R. W. Hyers, T. J. Rathz, J. R. Rogers, and D. S. Robinson, Phys. Rev. Lett. **93**, 037802 (2004).
[28]W. K. Luo, H. W. Sheng, F. M. Alamgir, J. M. Bai, J. H. He, and E. Ma, Phys. Rev. Lett. **92**, 145502 (2004).
[29]A. Posada-Amarillas and I. L. Garzón, Phys. Rev. B **53**, 8363 (1996).
[30]F. Spaepen, Nature (London) **408**, 781 (2000).
[31]P. R. ten Wolde, M. J. Ruiz-Montero, and D. Frenkel, Phys. Rev. Lett. **75**, 2714 (1995).
[32]X. Feng, Y. Ren-Hui, F. Liang, L. Lan-Xiao, and Z. Hong-Kai, Trans. Nonferrous Met. Soc. China **18**, 24 (2008).
[33]Y. Plevachuk, I. Egry, D. H.-M. J. Brillo, and I. Kaban, Int. J. Mater. Res. **98**, 107 (2007).
[34]A. F. Crawley, Int. Metall. Rev. **19**, 32 (1974).
[35]W. D. Drotning, in *Thermal Expansion 7*, edited by D. C. Larson (Plenum, New York, 1988), pp. 17–28.
[36]L. Fang, S. F. Zhang, F. Xiao, R. H. Yang, and K. Mukai, J. Alloys Compd. **493**, 465 (2010).
[37]J. Lill, C. Woodward, and D. Trinkle (unpublished).